Modeling transpiration with sun-induced chlorophyll fluorescence via water use efficiency and stomatal conductance

Huaize Feng[1], Tongren Xu[1], Xinlei He[1], Jingxue Zhao[1], Shaomin Liu[1]

[1] State Key Laboratory of Earth Surface Processes and Resource Ecology, School of Natural Resources, Faculty of Geographical Science, Beijing Normal University, Beijing 100875, China

Key Points:

- SIF can be used to model transpiration via water use efficiency and stomatal conductance
- Mechanism models of SIF and transpiration outperformed linear model
- Air dryness has an important impact on the relationship between transpiration and SIF.

Abstract

Successfully applied in the carbon research area, sun-induced chlorophyll fluorescence (SIF) has raised the interest of researchers from the water research domain. However, the mechanism between SIF emitted by plants and transpiration (T) has not been fully explored. To improve the understanding of the relationship between SIF and T, we developed two SIF-T models, the WUE model and the conductance model, based on carbon-water coupling framework. Hourly data were used to build and validate the models we developed. Correlation analysis shows that the T modeled by our model outperforms the traditional empirical linear model with higher R^2 and lower RMSE. The models we built further show the potential and mechanism in estimating water flux by SIF.

1 Introduction

Evapotranspiration (ET) is not only a pipeline of the water cycle in the air but also an important influence factor of energy balance as a carrier of latent heat. Previous works indicated transpiration (T) occupies a dominant position in evapotranspiration [*Good et al.*, 2015; *Jasechko et al.*, 2013]. In some ecosystems, T could reach 95% of the total ET [*Stoy et al.*, 2019]. T is also closely coupled with the carbon plant productivity [*Kool et al.*, 2014]. Therefore, an accurate understanding of the

fenghuaize@mail.bnu.edu.cn

spatiotemporal changes of T is crucial for understanding the substance and energy interactions between the land surface and the atmosphere.

In this century, Sun-induced chlorophyll fluorescence (SIF) renewed the gross primary production (GPP) estimation from ground to space [*Frankenberg and Berry*, 2018; *Ryu et al.*, 2019; *Schimel et al.*, 2019]. Considering the connection between photosynthesis and transpiration, SIF may serve as a pertinent constrain estimates for transpiration. [*Alemohammad et al.*, 2017; *Jonard et al.*, 2020]. Recently, Empirical analysis based on ground and remote sensing SIF observation showed SIF is strongly related to T, [*Lu et al.*, 2018] reconstructed the full band SIF and exploit the capacity of individual SIF bands and their combinations for deriving T with empirical linear regression and Gaussian Process Regression model at Harvard Forest. [*Pagán et al.*, 2019] used radiation corrected GOME-2 SIF observations to diagnose transpiration efficiency understood as the ratio between transpiration and potential evaporation worldwide. [*Maes et al.*, 2020] investigated the empirical link between SIF and T using satellite SIF (GOME-2 and OCO-2) and SCOPE model at sites from FLUXNET. However, the studies mentioned above relate T with SIF empirically, not mechanistically. SIF is the light signal from the excited chlorophyll a molecules after absorption of photosynthetically active radiation. The information about the electron transport (J) from photosystem II to photosystem I contained in SIF makes the signal a powerful tool to predict GPP [*Gu et al.*, 2019; *Köhler et al.*, 2018; *Zhang et al.*, 2014]. Furthermore, the essential of understanding the SIF-T relationship should lie in the coupling between the carbon and water cycles.

The carbon and water cycles between the biosphere and atmosphere are strongly coupled [*Gentine et al.*, 2019]. The trade-off between photosynthesis and water vapor loss is arguably the most central constraint on plant function [*Wolz et al.*, 2017]. Water-use efficiency (WUE) and stomatal conductance (gs, or canopy conductance, gc) are two key metrics of carbon - water coupling. WUE is defined as the amount of carbon assimilated relative to water use [*Leakey et al.*, 2019]. [*Maes et al.*, 2020] reported WUE and related variables show a most important impact on the SIF-T relation. Plants take in carbon dioxide and breath out water through stomata simultaneously. Stomata played a key role in the carbon-water coupling, even the whole Earth System [*Berry et al.*, 2010]. By analyzing the empirical link of SIF and canopy conductance, [*Shan et al.*, 2019] reported the empirically linear linkage between gs and SIF data from C3 forest, cropland, and grassland ecosystems, and T calculated by SIF-based conductance agreed well with ET observed by flux towers. However, it is still unclear how can WUE and gs be used to model T by SIF mechanistically.

In this paper, two carbon-water coupling indicators: water use efficient and stomatal conductance are introduced to clarify the physical relevance between SIF and T. Using the concept of these two indicators, two mechanism SIF-T models are built and tested based on hourly ground observation from four sites, including two C4 and two C3 sites. The results are expected to improve our understanding of the link between SIF and T.

2 Materials and Methods

2.1 Materials

SIF and corresponding observation (eg. weather variables, flux data, and vegetation indexes) are acquired at four sites including two maize field sites (Daman from Heihe river basin, China, DM; Huailai from Haihe river basin, China, HL), one temperate deciduous forest site (Harvard Forest from AmeriFlux network, US, HF) and a subalpine conifer forest (Niwot Ridge from AmeriFlux network, US, NR). The characteristics of these sites are summarized in Table 3. The SIF measurements of DM and HL sites (760 nm) were conducted using a tower-based automatic

fenghuaize@mail.bnu.edu.cn

measurement system named "SIFSpec" [*Du et al.*, 2018] and retrieved using the 3FLD method [*Liu et al.*, 2020]. The SIF data (745- to 758-nm) of NR were from a scanning spectrometer (PhotoSpec) on the top of the 26 meters tower. SIF data in winter were abandoned in this study because the subalpine trees at the NR site undergone significant physiological stress during the cold climate [*Magney et al.*, 2019]. The SIF data of HF were retrieved from FluoSpec deployed about 5 m above the canopy on the top of a tower and extracted by spectral fitting methods at 760 nm [*Yang et al.*, 2015].

Leaf area index (LAI) of all four sites was acquired from the MCD15A3H dataset with 4-day and 500 m temporal-spatial resolution [*Myneni et al.*, 2015] and interpolated to hourly scale on Google Earth Engine [*Gorelick et al.*, 2017]. Gross primary production (GPP) was separated from net ecosystem exchange (NEE) following [*Reichstein et al.*, 2005] and [*Lasslop et al.*, 2010] via the REddyProcWeb online tool (https://www.bgcjena.mpg.de/bgi/index.php/Services/REddyProcWeb). One hour before the rainfall and six hours after the rainfall data were excluded to minimize the influence of canopy interception.

T modeled by SIF is evaluated by T_{Zhou} partitioned from ET. [*Zhou et al.*, 2014] proposed an index called underlying water-use efficiency (uWUE) by combining the optimal stomatal behavior model with Fick's law. At the leaf scale, uWUE is defined as:

$$\mathrm{uWUE_l} = \frac{\mathrm{GPP} \times \sqrt{\mathrm{VPD}}}{\mathrm{T}} \tag{1}$$

Where VPD is the vapor pressure deficit, which is calculated from air temperature and relative humidity of air. At the ecosystem scale, uWUE is written as:

$$\mathrm{uWUE_a} = \frac{\mathrm{GPP} \times \sqrt{\mathrm{VPD}}}{\mathrm{ET}} \tag{2}$$

fenghuaize@mail.bnu.edu.cn

When water flux from the surface is fully occupied by transpiration from plants, $uWUE_a$ reaches its potential value $uWUE_p$. The $uWUE_p$ is assumed to be equaling to $uWUE_l$ and can be captured by the 95-quantile regression analysis of $uWUE_a$. Then T can be derived by:

$$T_{Zhou} = \frac{GPP \times \sqrt{VPD}}{uWUE_p} \quad (3)$$

This method was developed based on flux tower data of 14 sites, including the HF site, and successfully applied to Heihe River Basin [*Zhou et al.*, 2018], including the DM site. Especially, at the DM site, T/ET estimated by the uWUE method agreed with the isotope method well during the peak growing season [*Bai et al.*, 2019].

2.2 WUE Model

SIF can be represented in the form of light use efficiency (LUE) model:

$$SIF = APAR\ \Phi_F\ \Omega_c \quad (4)$$

where APAR stands the photosynthetically active radiation absorbed by photosynthetic pigments, Φ_F is the fluorescence quantum yield and Ω_c is the probability of SIF photon escaping from the canopy. Combined Eqn 4 with the LUE model of GPP (Eqn 5). We can obtain a linear model between SIF and GPP (Eqn 3):

$$GPP = APAR\ LUE \quad (5)$$

$$GPP = SIF \frac{LUE}{\Phi_F\ \Omega_c} \quad (6)$$

where LUE is the light-use-efficiency. A series of papers have reported the linear relationship between SIF and GPP by comparing GPP with satellite remote sensing SIF [*Guanter et al.*, 2014; *Li et al.*, 2018; *Sun et al.*, 2017] and field-based SIF observation [*Liu et al.*, 2017; *Magney et al.*, 2019; *Yang et al.*, 2015]. Based on these works, the factor $\frac{LUE}{\Phi_F \times \Omega_c}$ can be set as a constant for a specific plant type, and GPP can be calculated by SIF directly. For C3 and C4 plants, WUE is relatively stable. Many works derived T from GPP by treating WUE as a constant value during certain period [*Scott and Biederman*, 2017; *Yang et al.*, 2015]. Under this assumption T can be calculated by SIF via the following equation:

$$\mathrm{GPP_{linear}} = \mathrm{k1\ SIF} \tag{7}$$

$$\mathrm{T_{linear}} = \mathrm{k2\ GPP_{linear}} \tag{8}$$

where k1, k2 are two parameters denoting $\frac{\mathrm{LUE}}{\Phi_F \times \Omega_c}$ and WUE respectively. Eqn 8 is the theory base of the empirical linear relationship between SIF and T.

However, WUE is strongly affected by the dryness of air from leaf to ecosystem scale. The relationship between GPP and T improved significantly by incorporating the effects of VPD from diurnal to annual time scales [*Beer et al.*, 2009; *Zhou et al.*, 2014]. Moreover, [*Jonard et al.*, 2020] pointed out the atmospheric demand for water helps explaining a lot variability in the SIF–T relationship at the ecosystem scale. Here we proposed a WUE model:

$$\mathrm{GPP_{WUE}} = \mathrm{k3\ SIF} \tag{9}$$

$$\mathrm{T_{WUE}} = \mathrm{k4\ VPD^{k5}\ GPP_{WUE}} \tag{10}$$

where k3 is a parameter like k1. k4 is a parameter concluding information on water-use efficiency. k5 quantifies of the non-linear effect of VPD on k4 [*Lin et al.*, 2018]. In this work, the VPD of air is used to describe the aridity stress at the canopy scale.

2.3 Conductance Model

Though the linear SIF-GPP relationship looks simple, the mechanism of the parameter LUE in Eqn 3 is complex. Φ_f and Ω_c are relatively stable value [*Guanter et al.*, 2014; *Tol et al.*, 2014], and LUE is often calculated by reducing potential LUE using several environmental factors, such as temperature, soil moisture [*Yuan et al.*, 2007]. Previous work had also reported the hyperbolic relationship between SIF and GPP [*Damm et al.*, 2015; *Zhang et al.*, 2020]. Therefore, the relationship between SIF and GPP is far more complicated than linear. As mentioned above, the link between SIF and GPP is because of the close relationship between SIF and electron transport rate (J). Benefit from the carbon-pump mechanism, the GPP of C4 plants is linearly related to J [*Gu et al.*, 2019]. For C4 plants, GPP can be derived by:

$$\mathrm{J} = \mathrm{a}\ \mathrm{q_L}\ \mathrm{SIF} \tag{11}$$

$$\mathrm{GPP_{gs}} = \mathrm{J}/4 = \frac{\mathrm{a}\ \mathrm{q_L}\ \mathrm{SIF}}{4\Omega_\mathrm{c}} \tag{12}$$

a is an empirical factor supposed to be a constant under ideal environments, q_L is the fraction of open Photosynthesis II reaction centers, indicating the 'traffic jam' in the electron transport pathway from Photosystem II to Photosystem I. Note that, the Eqn 11 is designed for broadband SIF for PSII. In this paper, single NIR band SIF is used instead by assuming a linear relationship between single-band SIF and full band SIF. q_L ranges from 0-1 and decreases with increased PAR [*Baker*, 2008; *Gu et al.*, 2019]. In this paper, q_L is derived by:

$$\mathrm{q_L} = \exp(-\beta \mathrm{PAR}) \tag{13}$$

β is a parameter denoting the sensitivity of q_L to the illumination. Due to data restrictions, Ω_c for the near-infrared band SIF was set as a constant in our study. gs for C4 plants is derived by inserting Eqn into the famous Ball-Berry model [*Ball et al.*, 1987]:

$$\mathrm{gs} = \mathrm{m}\ \frac{\mathrm{a}\ \mathrm{q_L}\ \mathrm{SIF}}{4\Omega_\mathrm{c}} \mathrm{Rh}/\mathrm{C_a} + \mathrm{g_0} \tag{14}$$

Where m is an empirical slope parameter, which is often treated as a constant for a specific ecosystem [*Miner et al.*, 2017]. C_a is the ambient carbon dioxide concentration and g_0 is the minimum conductance which is set as 0. Lack of an efficient mechanism gathering CO_2 from the air, C3 plants much more rely on the stomata to absorb CO_2 for the Calvin cycle. For C3 plants, the relationship between SIF and GPP is also affected by the dark reactions [*Gu et al.*, 2019]:

$$\mathrm{GPP_{gs}} = \mathrm{a}\frac{\mathrm{C_i} - \Gamma^*}{4\mathrm{C_i} + 8\Gamma^*}\mathrm{q_L}\ \mathrm{SIF}\frac{1}{\Omega_\mathrm{c}} \tag{15}$$

C_i is the intercellular CO_2 concentration. Γ^* is the CO_2 compensation point in the absence of mitochondrial respiration, which can be set as a constant for specific plant type or calculated by air temperature [*Katul et al.*, 2010]. C_i in Eqn 10 can be eliminated by combining with Eqn 7 and Fick's law $\mathrm{GPP} = \mathrm{gs} \times (\mathrm{C_i} - \mathrm{C_a})$, then we have:

$$\mathrm{GPP_{gs}} = \mathrm{a}\frac{\mathrm{GPP/gs} + \mathrm{C_a} - \Gamma^*}{4(\mathrm{GPP/gs} + \mathrm{C_a}) + 8\Gamma^*}\mathrm{q_L}\ \mathrm{SIF}\frac{1}{\Omega_\mathrm{c}} \tag{16}$$

gs and GPP_{gs} can be solved under the constraining of the optimality theory of stomatal behavior. [*Cowan and GD*, 1977; *Katul et al.*, 2010; *Way et al.*, 2014]. According to this theory, plants tend to adapt stomata to minimize the cost of water while maximizing carbon assimilation:

$$\mathrm{f(gs)} = \mathrm{GPP} - \lambda\,\mathrm{ET} \approx\ \mathrm{GPP} - 1.6\lambda\,\mathrm{gs}\,\mathrm{VPD/P} \tag{17}$$

$$\delta\mathrm{f(gs)}/\delta(\mathrm{gs}) = 0 \tag{18}$$

λ represents the marginal water cost of carbon assimilation. P is the air pressure. If we incorporate Eqn 16, 17, and 18, gs can be expressed as the function $\boldsymbol{\mathcal{F}}$ of SIF, q_L, λ, Γ, VPD and C_a:

$$\mathrm{gs} = \boldsymbol{\mathcal{F}}(\mathrm{SIF}, \mathrm{q_L}, \lambda, \Gamma, \mathrm{VPD}, \mathrm{C_a})$$

$$= -\frac{\mathrm{a\ SIF\ q_L}(4\Gamma - \mathrm{C_a})}{4(2\Gamma + \mathrm{C_a})^2} + \frac{\mathrm{a\ SIF\ q_L}(2\Gamma + \mathrm{C_a} - 3.2\lambda\,\mathrm{VPD})\sqrt{3.2\lambda\,\mathrm{VPD}\,\Gamma(\mathrm{C_a} - \Gamma)(2\Gamma + \mathrm{C_a} - 1.6\mathrm{VPD}\lambda)}}{6.4\lambda\,\mathrm{VPD}(2\Gamma + \mathrm{C_a})^2(2\Gamma + \mathrm{C_a} - 1.6\lambda\,\mathrm{VPD})} \tag{19}$$

Finally, with SIF-based gs, T can be calculated by the two-source Penman-Monteith method [*Leuning et al.*, 2008]:

$$\mathrm{Ac} = \mathrm{Rn} \times [1 - \exp(-0.5\mathrm{LAI})/\cos(\mathrm{SZA})] \tag{20}$$

$$\mathrm{T_{gs}} = \frac{\Delta\,\mathrm{Ac} + \rho\,\mathrm{C_p}\,\mathrm{VPD}\,\mathrm{ga}}{\Delta + \gamma\left(1 + \frac{\mathrm{ga}}{\mathrm{gs}}\right)} \tag{21}$$

Eqn 20 is the simple one-dimensional Beer's law model. Ac is the available energy of the canopy layer, Rn is net radiation, LAI is the leaf area index and SZA is the sun zenith angle. For Eqn 21, where Δ is the rate of change of vapor pressure with temperature, γ is the psychrometric constant, C_p is the specific heat of air; ρ is the density of liquid water and ga is aerodynamic conductance.

2.3 Model Calibration

Parameters of both the WUE model and the conductance model need to be calibrated. GPP and the water balance framework are used here to constrain the models. Total ET observed by eddy covariance measurement is composed of plant transpiration (T) and soil evaporation (LEs):

$$\mathrm{LE} = \mathrm{T} + \mathrm{LEs} \tag{22}$$

Considering the nonlinearity and complicity of the models, the shuffled complex evolution (SUE-UA) algorithm [*Duan et al.*, 1994] is employed to fit parameters by maximizing the cost function G:

$$\mathrm{G} = 0.4\mathrm{NSE}(\mathrm{GPP_{ob}}, \mathrm{GPP_{model}}) + 0.6\mathrm{NSE}(\mathrm{LE_{ob}}, \mathrm{LE_{model}}) \tag{23}$$

where NSE is the Nash-Sutcliffe efficiency coefficient. The subscript $_{ob}$ means observed values and variables with a subscript $_{model}$ mean values are derived by models described above. All model estimations and statistical analyses were performed with Python 3.8.3 [*Herman and Usher*, 2017; *Houska et al.*, 2015]. The description and calculation of all variables mentioned above are listed in Table 2.

fenghuaize@mail.bnu.edu.cn

3 Results

3.1 Performance of SIF- T model

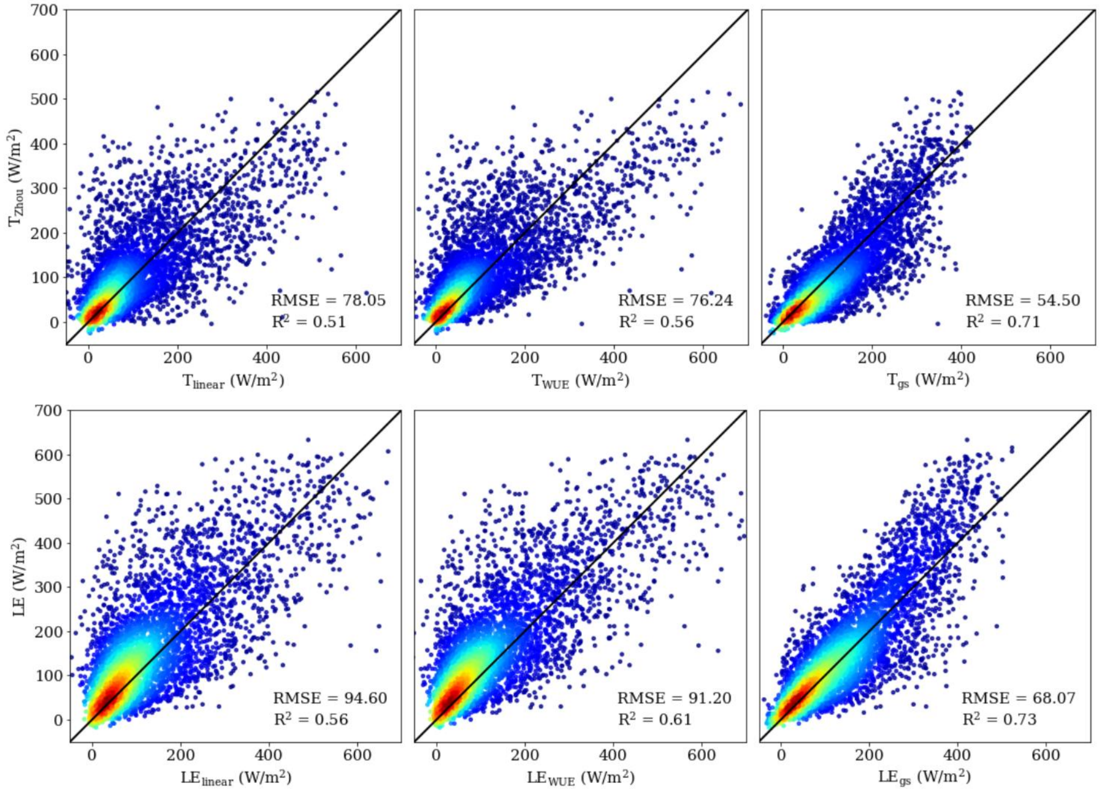

Figure 1. Relationship of T modeled by SIF and reference latent heat (Hourly). Colors indicate the density of points (from sparse to dense: blue to red). R^2 denotes the coefficient of determination. The unit of root-mean-square deviation (RMSE) is W/m^2.

Scatter plots between reference T_{Zhou} and T modeled by SIF are shown in Fig1 (upper row). In general, both the WUE method and the conductance method improve the ability of SIF in modeling T. Compared with simple linear regression with R^2 = 0.51 and RMSE = 78.05 W/m^2, the WUE model has R^2 = 0.56 and RMSE = 76.24 W/m^2, while the conductance model has the highest R^2 = 0.71 and much lower RMSE = 54.50 W/m^2. The linear model and the WUE model tend to overestimate T at the high values area, while most points of T_{gs} fall near the 1:1 line.

The reference T_{Zhou} may have considerable uncertainty. Plants do not always keep a specific response (square root) to VPD like described in Zhou's method. Moreover, in some ecosystems, the soil evaporation can not be ignored even in the peak growing season [*Li et al.*, 2019; *Stoy et* *al.*, 2019]. Here we also compared the LE derived by three SIF-T models with LE observed by eddy covariance in Fig1 (lower row). The linear model, WUE model and conductance model have R^2 = 0.56, 0.61 and 0.73 and RMSE = 94.60, 91.20 and 68.07 W/m^2 respectively. Same as compared with T_{Zhou}, the conductance model outperforms the other two models with the highest coefficients of determination and the lowest RMSE. The WUE model also has better performance than the widely used linear model.

The performance of three models at different sites is shown in Table 4. When compared to T_{Zhou}, the conductance model shows the best performance at DM and HF sites with much higher R^2 = 0.84, 0.62, and lower RMSE = 47.98, 77.43 W/m^2 respectively. The linear model shows the best performance with R^2 = 0.58 and RMSE = 50.94 W/m^2 at the HL site. The WUE model outperforms other models at the NR site. When compared to LE observed by eddy covariance, the conductance model shows outstanding performance at all four sites. Besides, the WUE model has the lowest RMSE = 67.38 W/m^2 at the NR site.

3.2 Sensitivity analysis of variables in two models

To explore what influences the relationship between SIF and T, we analyzed the sensitivity of variables in WUE and conductance models. For the WUE model, the scatterplot between SIF and T_{WUE} is shown in Fig. T is the product of SIF and VPD in the WUE model, which means SIF and VPD interact with each other closely and the effect of the SIF is modified by the VPD. The parameter k5 for four sites are 0.33, 0.45, 0.97, and 0.02 respectively. With the increase of VPD, the slopes of SIF-T get steeper and points get denser, while in the low VPD condition, the points are relatively sparse, which indicates the relationship between SIF and T is more linear under high VPD. Especially we find the relation between SIF and T at the HF site is not sensitive to the VPD.

fenghuaize@mail.bnu.edu.cn

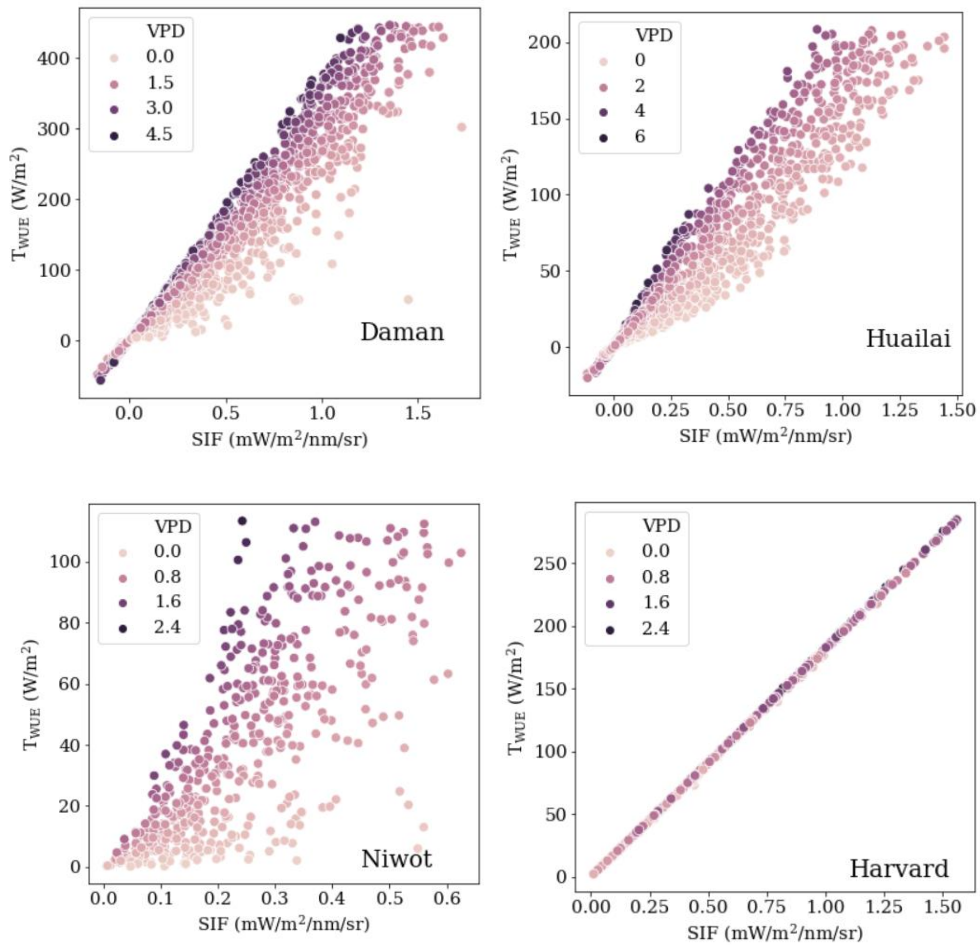

Figure 2. Scatter plot between SIF and T modeled by the WUE method. The vapor pressure deficit (VPD) has the unit kPa.

Atmospheric dryness is also important in modeling the stomatal behavior by SIF. For C4 plants, relative humidity is used to describe the response of stomatal conductance to air dryness in the empirical Ball Berry model. For C3 plants, we investigated the sensitivities of different variables in the gs model $\mathcal{F}$ by RBD-FAST-Random Balance Designs Fourier Amplitude Sensitivity Test [*Tarantola et al.*, 2006]. According to Fig 3, $\mathcal{F}$ is sensitive to VPD, λ, SIF, and q_L. VPD exhibits the highest first-order sensitivities with values equaling 0.15, which is much higher than SIF with value 0.07. The marginal water use efficiency λ also plays an important role in $\mathcal{F}$ with sensitivity value equaling 0.14. The fraction of open Photosynthesis II reaction centers q_L is as important as SIF (1^{st}-order sensitivity: 0.07), which is due to the electron transport rate J

fenghuaize@mail.bnu.edu.cn

is the product of SIF and q_L (Eqn 1). What's more, the gs model is not sensitive to air temperature and ambient carbon dioxide concentration. However, VPD used here is calculated by temperature and relative humidity of the air. The temperature information contained in VPD (R^2 of Ta-VPD is 0.48) may impair the role of air temperature in the model. In this paper, q_L is calculated by a simple empirical equation of PAR. In fact, q_L is also related to the dark reaction but poorly studied [*Baker*, 2008; *Gu et al.*, 2019]. More researches about q_L will improve our understanding of the relationship between SIF and J, further the SIF-GPP and SIF-T relationships.

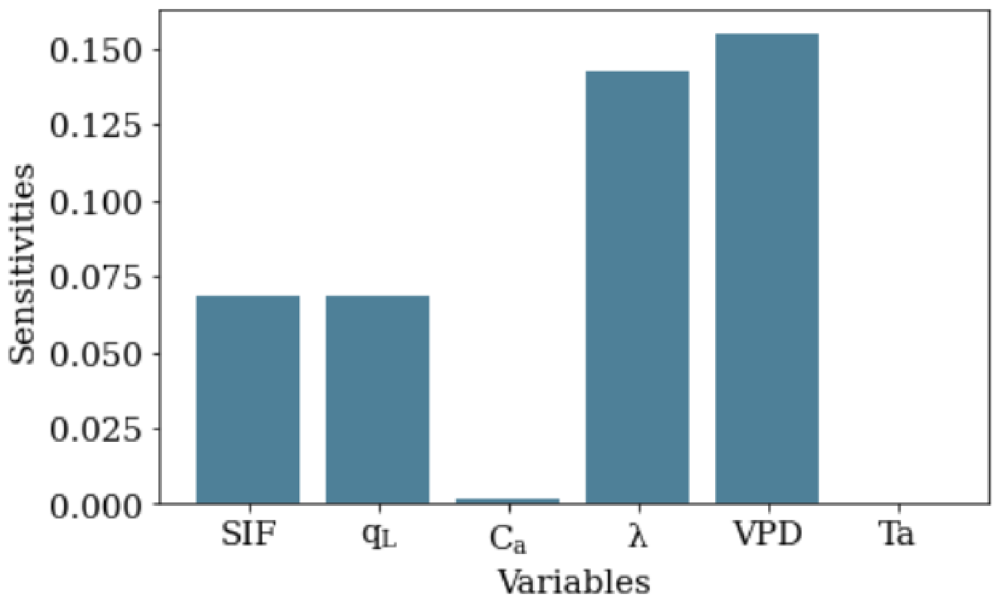

Figure 3. Sensitivity analysis of variables in the stomatal conductance model $\mathcal{F}$ of C3 plants. The height of bars shows the 1st order sensitivities of different variables.

4 Discussion

Above all, the assumptions of carbon-water coupling may affect our results. Comparing with the linear model, though the influence of VPD on water-use efficiency is included in the WUE model, soil moisture, hydraulic conductance, and other environmental variables can influence water-use efficiency independently [*Leakey et al.*, 2019; *Lin et al.*, 2015; *Liu et al.*, 2020]. For the conductance model, plants under stress or competition tend to change the optimal stomatal conductance behavior [*Wolf et al.*, 2016]. The carbon-water economy is also influenced by traits of plants and environmental variables [*Bloom et al.*, 1985; *Buckley et al.*, 2017]. This concept is out of the scope of this paper, but a more physiologically based water-carbon coupling framework will improve the models from the bottom up.

Due to the absence of direct measurements of transpiration during the research period, three models were calibrated by the water budget balance framework, which might introduce uncertainty to parameters, further the performance of the models. Net radiation is separated into energy intercepted by canopy and soil available energy by 1D Beer's law. The simple structure of Beer's law can introduce great uncertainty, especially for heterogeneity canopy and plants with leaves highly anisotropic leaves in the azimuthal direction [*Ponce De León and Bailey*, 2019]. In the conductance model, canopy available energy is also used to estimate transpiration in the two-source Penman-Monteith model. So, the conductance model is more sensitive to the partition of energy, in other words, suffers more uncertainty from Beer’s law. Uncertainty of input data might also affect our results. Firstly, VPD in the air was used to assess the aridity stress by assuming the canopy and the atmosphere are fully coupled. Yet, ecosystems (DM, HL, and HF) with dense closed canopy tend to decouple from the air [*De Kauwe et al.*, 2017; *Li et al.*, 2019; *Lin et al.*, 2018]. As both the WUE model and conductance model shows great sensitivity to VPD, using VPD at the leaf scale could help to improve the performance of the SIF-T relationship. Secondly, SIF data from four sites are measured by different instruments and derived by different methods as mentioned above. Moreover, the FOV and height of the observation systems vary among sites. So, it is difficult to derive universal parameters for all sites. Last but not the least, the canopy-scale SIF was directly used to model transpiration due to data restriction. Nevertheless, recent papers indicated the relationship between SIF and GPP is strongly affected by the structure of the canopy

[*Liu et al.*, 2019; *Zeng et al.*, 2019]. We suggest downscaling of SIF from the canopy scale to the photosystem scale may improve the performance of the model.

Data from four sites were used to test the performance of the models. It is inadequate to show the real potential of two models. With more and more in-situ observations from different ecosystems, understanding of the underlying mechanism between SIF and T will be deepened. Recently, SIF products with higher temporal-spatial resolution from different satellites, different bands [*Du et al.*, 2018; *Köhler et al.*, 2018; *Köhler et al.*, 2020], and derivative products based on machine learning [*Li and Xiao*, 2019; *Ma et al.*, 2020; *Yu et al.*, 2019; *Zhang et al.*, 2018] became available. WUE model and conductance model can be easily combined with remote sensing ET/T model like TSEB [*Norman et al.*, 1995; *Song et al.*, 2016] and PML ([*Zhang et al.*, 2019] or used for assimilating SIF into a land surface model. With these data and models in this paper, estimating T via SIF at the big scale becomes promising.

5 Conclusion

In this study, in-situ hourly SIF and corresponding meteorological variables, eddy covariance observation and vegetation indexes at C3 and C4 sites were collected. Two SIF-T models based on water-use efficiency and stomatal conductance were developed and tested upon this data. Both models outperformed simple linear analysis with higher R^2 and lower RMSE. Our results indicate the SIF-T relationship depends on air dryness. These two carbon-water coupling models can be easily combined with state-of-the-art remote sensing models or land process models. Moreover, with the emergency of high temporal-spatial resolution SIF data, SIF will not only be a powerful proxy for carbon flux but also water flux at the planetary scale.

fenghuaize@mail.bnu.edu.cn

Non-peer reviewed EarthArXiv preprint
【This manuscript has not been submitted to any journal and not under any peer review yet】

Table 1. Summary of the stations used to build models.

	Latitude	Longitude	Period	Land Cover	Reference
DM	100.37°E	38.85°N	2017.6 – 2017.9; 2018.6 – 2018.9	Maize (C4)	[*Liu et al.*, 2018; *Liu et al.*, 2019]
HL	115.78°E	40.33°N	2017.7 – 2017.10; 2018.7 – 2018.10	Maize (C4)	[*Liu et al.*, 2013; *Liu et al.*, 2019]
NR	105.55°W	40.03°N	2017.6-2017.9; 2018.6-2018.7	Mixed temperate forest (C3)	[*Burns et al.*, 2015; *Magney et al.*, 2019]
HF	72.17° W	42.54°N	2013.6-2013.11	Evergreen needle leaf forest(C3)	[*Munger W*, 2020; *Yang et al.*, 2015]

Table 2. Input and intermediate variables. AWS denotes auto weather station. FAO indicates the computation methods of the variable is from http://www.fao.org.

Variables	Unit	Description	Source	Remarks
C_a	μmol/mol	ambient CO2 concentration	Observation	Eddy covariance
C_p	J/Kg/K	specific heat of air	1013	FAO
LEs	W/m^2	Soil evaporation	$\frac{f\Delta(Rn - A_c)}{\Delta + \gamma}$	[*Fisher et al.*, 2008]
f	-	Soil evaporation constraint	$SM/(SM_{max} - SM_{min})$	-
ga	m/s	Aerodynamic conductance	$\frac{1}{v/(u*)^2 + 6.2(u*)^{-2/3}}$	[*Monteith and Unsworth*, 2013]
GPP_{ob}	$\mu mol/m^2/s$	Gross primary production	Separated from NEE observed by eddy covariance	[*Lasslop et al.*, 2010; *Reichstein et al.*, 2005]
LE	W/m^2	Latent heat	Observation	Eddy covariance
PAR	W/m^2	photosynthetically active radiation	Observation	AWS
P	kPa	Air Pressure	Observation	AWS
q_L	-	Fraction of open Photosynthesis II reaction centers	$\exp(-\beta\ PAR)$	This paper
Rh	-	Relative humidity	Observation	AWS
Rn	W/m^2	Net radiation	Observation	AWS
SIF	$mW/m^2/sr/nm$	Sun-induced chlorophyll fluorescence	Observation	-
SM	%	Soil moisture	Observation	Thermal Dissipation Probe
Ta	°C	Air temperature	Observation	AWS

fenghuaize@mail.bnu.edu.cn

u*	m/s	Friction Velocity	Observation	Eddy covariance
v	m/s	Wind speed	Observation	AWS
VPD	kPa	Vapor pressure deficit	$(100 - \mathrm{Rh})/100 \times 0.6108 \times \exp(17.27\ \mathrm{Ta}/(\mathrm{Ta} + 237.3))$	FAO
Δ	kPa/K	Slope of saturation vapor pressure curve	$(2503 \exp(17.27\ \mathrm{Ta}/(\mathrm{Ta} + 237.3)))/((\mathrm{Ta} + 237.3)^2)$	FAO
γ	kPa/K	psychrometric constant	$0.665 \times 0.001\mathrm{P}$	FAO
Γ	μmol/mol	CO2 compensation point in the absence of mitochondrial	$36.9 + 1.18(\mathrm{Ta} - 25) + 0.036(\mathrm{Ta} - 25)^2$ for C3; 0 for C4	[*Katul et al.*, 2010]
ρ_a	kg/m^3	Air density	$1.292 - 0.00428\ \mathrm{Ta}$	FAO

Table 3. Parameters needed to be calibrated.

	Parameter	Lower	Upper	Reference
Linear model	K1	5	50	[*Liu et al.*, 2017; *Sun et al.*, 2017]
	K2	3	50	[*Huang et al.*, 2016]
WUE model	K3	5	50	[*Liu et al.*, 2017; *Sun et al.*, 2017]
	K4	3	30	[*Zhou et al.*, 2015]; This paper
	K5	0	1	[*Lin et al.*, 2018]
Conductance model (C4)	β	0	0.001	This paper; [*Gu et al.*, 2019]
	a	10	300	This paper
	m	2.5	8.8	[*Miner et al.*, 2017]
Conductance model (C3)	β	0	0.01	This paper; [*Gu et al.*, 2019; *Katul et al.*, 2010]
	a	10	300	This paper
	λ	10	200	[*Cowan and GD*, 1977; *Katul et al.*, 2010]

Table 4. Coefficient of determination (R^2) and root mean square error (RMSE) at different sites. Best values are marked with the bold font.

	Reference	**DM**		**HL**		**NR**		**HF**	
		R^2	RMSE	R^2	RMSE	R^2	RMSE	R^2	RMSE
T_{linear}	T_{Zhou}	0.46	104.25	**0.58**	**50.94**	0.49	35.32	0.45	70.66
T_{WUE}		0.55	99.11	0.55	53.66	**0.69**	**29.26**	0.45	71.80

T_{gs}		**0.84**	**47.98**	0.57	54.79	0.46	41.27	**0.62**	**77.43**
LE_{linear}		0.56	119.97	0.52	67.69	0.27	68.69	0.44	81.92
LE_{WUE}	LE	0.55	114.20	0.55	66.71	0.36	**67.38**	0.44	84.87
LE_{gs}		**0.87**	**69.36**	**0.60**	**64.53**	**0.40**	68.82	**0.55**	**70.71**

References:

Alemohammad, S. H., et al. (2017), Water, Energy, and Carbon with Artificial Neural Networks (WECANN): a statistically based estimate of global surface turbulent fluxes and gross primary productivity using solar-induced fluorescence, *BIOGEOSCIENCES*, *14*(18), 4101-4124.

Bai, Y., et al. (2019), Quantifying plant transpiration and canopy conductance using eddy flux data: An underlying water use efficiency method, *AGR FOREST METEOROL*, *271*, 375-384.

Baker, N. R. (2008), Chlorophyll Fluorescence: A Probe of Photosynthesis In Vivo, *ANNU REV PLANT BIOL*, *59*(1), 89-113.

Ball, J. T., et al. (1987), A model predicting stomatal conductance and its contribution to the control of photosynthesis under different environmental conditions, in *Progress in photosynthesis research*, edited, pp. 221-224, Springer.

Beer, C., et al. (2009), Temporal and among-site variability of inherent water use efficiency at the ecosystem level, *GLOBAL BIOGEOCHEM CY*, *23*(2), n/a-n/a.

Berry, J. A., et al. (2010), Stomata: key players in the earth system, past and present, *CURR OPIN PLANT BIOL*, *13*(3), 232-239.

Bloom, A. J., et al. (1985), Resource limitation in plants-an economic analogy, *Annual review of Ecology and Systematics*, *16*(1), 363-392.

Buckley, T. N., et al. (2017), Optimal plant water economy, *Plant, Cell & Environment*, *40*(6), 881-896.

Burns, S. P., et al. (2015), The influence of warm-season precipitation on the diel cycle of the surface energy balance and carbon dioxide at a Colorado subalpine forest site, *BIOGEOSCIENCES*, *12*(23), 7349-7377.

Cowan, I. R., and F. GD (1977), Stomatal function in relation to leaf metabolism and environment.

Damm, A., et al. (2015), Far-red sun-induced chlorophyll fluorescence shows ecosystem-specific relationships to gross primary production: An assessment based on observational and modeling approaches, *REMOTE SENS ENVIRON*, *166*, 91-105.

De Kauwe, M. G., et al. (2017), Ideas and perspectives: how coupled is the vegetation to the boundary layer? *BIOGEOSCIENCES*, *14*(19), 4435-4453.

Du, S., et al. (2018), Retrieval of global terrestrial solar-induced chlorophyll fluorescence from TanSat satellite, *SCI BULL*, *63*(22), 1502-1512.

Duan, Q., et al. (1994), Optimal use of the SCE-UA global optimization method for calibrating watershed models, *J HYDROL*, *158*(3-4), 265-284.

Fisher, J. B., et al. (2008), Global estimates of the land‐atmosphere water flux based on monthly AVHRR and ISLSCP-II data, validated at 16 FLUXNET sites, *REMOTE SENS ENVIRON*, *112*(3), 901-919.

Frankenberg, C., and J. Berry (2018), Solar induced chlorophyll fluorescence: Origins, relation to photosynthesis and retrieval.

Gentine, P., et al. (2019), Coupling between the terrestrial carbon and water cycles—a review, *ENVIRON RES LETT*, *14*(8), 83003.

Good, S. P., et al. (2015), WATER RESOURCES. Hydrologic connectivity constrains partitioning of global terrestrial water fluxes, *SCIENCE*, *349*(6244), 175-177.

Gorelick, N., et al. (2017), Google Earth Engine: Planetary-scale geospatial analysis for everyone, *REMOTE SENS ENVIRON*, *202*, 18-27.

Gu, L., et al. (2019), Sun-induced Chl fluorescence and its importance for biophysical modeling of photosynthesis based on light reactions, *NEW PHYTOL*, *223*(3), 1179-1191.

Guanter, L., et al. (2014), Global and time-resolved monitoring of crop photosynthesis with chlorophyll fluorescence, *Proceedings of the National Academy of Sciences*, *111*(14), E1327-E1333.

Herman, J., and W. Usher (2017), SALib: an open-source Python library for sensitivity analysis, *Journal of Open Source Software*, *2*(9), 97.

Houska, T., et al. (2015), SPOTting model parameters using a ready-made python package, *PLOS ONE*, *10*(12), e145180.

Huang, M., et al. (2019), Air temperature optima of vegetation productivity across global biomes, *NAT ECOL EVOL*, *3*(5), 772-779.

Jasechko, S., et al. (2013), Terrestrial water fluxes dominated by transpiration, *NATURE*, *496*(7445), 347-350.

Jonard, F., et al. (2020), Value of sun-induced chlorophyll fluorescence for quantifying hydrological states and fluxes: Current status and challenges, *AGR FOREST METEOROL*, *291*, 108088.

Katul, G., et al. (2010), A stomatal optimization theory to describe the effects of atmospheric CO2 on leaf photosynthesis and transpiration, *ANN BOT-LONDON*, *105*(3), 431-442.

Köhler, P., et al. (2018), Global Retrievals of Solar‐Induced Chlorophyll Fluorescence With TROPOMI: First Results and Intersensor Comparison to OCO‐2, *GEOPHYS RES LETT*, *45*(19), 10, 410-456, 463.

Köhler, P., et al. (2020), Global Retrievals of Solar‐Induced Chlorophyll Fluorescence at Red Wavelengths With TROPOMI, *GEOPHYS RES LETT*, *47*(15).

Kool, D., et al. (2014), A review of approaches for evapotranspiration partitioning, *AGR FOREST METEOROL*, *184*, 56-70.

Lasslop, G., et al. (2010), Separation of net ecosystem exchange into assimilation and respiration using a light response curve approach: critical issues and global evaluation, *GLOBAL CHANGE BIOL*, *16*(1), 187-208.

Leakey, A., et al. (2019), Water Use Efficiency as a Constraint and Target for Improving the Resilience and Productivity of C3 and C4 Crops, *ANNU REV PLANT BIOL*, *70*, 781-808.

Leuning, R., et al. (2008), A simple surface conductance model to estimate regional evaporation using MODIS leaf area index and the Penman-Monteith equation, *WATER RESOUR RES*, *44*(10).

Li, X., et al. (2018), Solar-induced chlorophyll fluorescence is strongly correlated with terrestrial photosynthesis for a wide variety of biomes: First global analysis based on OCO-2 and flux tower observations, *GLOBAL CHANGE BIOL*, *24*(9), 3990-4008.

Li, X., et al. (2019), A simple and objective method to partition evapotranspiration into transpiration and evaporation at eddy-covariance sites, *AGR FOREST METEOROL*, *265*, 171-182.

Li, X., and J. Xiao (2019), A Global, 0.05-Degree Product of Solar-Induced Chlorophyll Fluorescence Derived from OCO-2, MODIS, and Reanalysis Data, *REMOTE SENS-BASEL*, *11*(5), 517.

Lin, C., et al. (2018), Diel ecosystem conductance response to vapor pressure deficit is suboptimal and independent of soil moisture, *AGR FOREST METEOROL*, *250-251*, 24-34.

Lin, Y., et al. (2015), Optimal stomatal behaviour around the world, *NAT CLIM CHANGE*, *5*(5), 459-464.

Liu, L., et al. (2017), Directly estimating diurnal changes in GPP for C3 and C4 crops using far-red sun-induced chlorophyll fluorescence, *AGR FOREST METEOROL*, *232*, 1-9.

Liu, S., et al. (2018), The Heihe Integrated Observatory Network: A Basin-Scale Land Surface Processes Observatory in China, *VADOSE ZONE J*, *17*(1), 180021-180072.

Liu, S. M., et al. (2013), Measurements of evapotranspiration from eddy-covariance systems and large aperture scintillometers in the Hai River Basin, China, *J HYDROL*, *487*, 24-38.

Liu, X., et al. (2019), Downscaling of solar-induced chlorophyll fluorescence from canopy level to photosystem level using a random forest model, *REMOTE SENS ENVIRON*, *231*, 110772.

Liu, X., et al. (2019), Atmospheric Correction for Tower-Based Solar-Induced Chlorophyll Fluorescence Observations at O2-A Band, *REMOTE SENS-BASEL*, *11*(3), 355.

Liu, X., et al. (2020), Improving the potential of red SIF for estimating GPP by downscaling from the canopy level to the photosystem level, *AGR FOREST METEOROL*, *281*, 107846.

Liu, Y., et al. (2020), Plant hydraulics accentuates the effect of atmospheric moisture stress on transpiration, *NAT CLIM CHANGE*, *10*(7), 691-695.

Lu, X., et al. (2018), Potential of solar-induced chlorophyll fluorescence to estimate transpiration in a temperate forest, *AGR FOREST METEOROL*, *252*, 75-87.

Ma, Y., et al. (2020), Generation of a Global Spatially Continuous TanSat Solar-Induced Chlorophyll Fluorescence Product by Considering the Impact of the Solar Radiation Intensity, *REMOTE SENS-BASEL*, *12*(13), 2167.

Maes, W. H., et al. (2020), Sun-induced fluorescence closely linked to ecosystem transpiration as evidenced by satellite data and radiative transfer models, *REMOTE SENS ENVIRON*, *249*, 112030.

Magney, T. S., et al. (2019), Mechanistic evidence for tracking the seasonality of photosynthesis with solar-induced fluorescence, *Proceedings of the National Academy of Sciences*, 201900278.

Miner, G. L., et al. (2017), Estimating the sensitivity of stomatal conductance to photosynthesis: a review, *Plant, Cell & Environment*, *40*(7), 1214-1238.

Monteith, J., and M. Unsworth (2013), Principles of environmental physics: plants, animals, and the atmosphere.

Munger W, W. S. (2020), Canopy-Atmosphere Exchange of Carbon, Water and Energy at Harvard Forest EMS Tower since 1991. Harvard Forest Data Archive: HF004., edited.

Myneni, R., et al. (2015), MCD15A3H MODIS/Terra+ Aqua Leaf Area Index/FPAR 4-day L4 Global 500m SIN Grid

V006., edited.

Norman, J. M., et al. (1995), Source approach for estimating soil and vegetation energy fluxes in observations of directional radiometric surface temperature, *AGR FOREST METEOROL*, *77*(3-4), 263-293.

Pagán, B., et al. (2019), Exploring the Potential of Satellite Solar-Induced Fluorescence to Constrain Global Transpiration Estimates, *REMOTE SENS-BASEL*, *11*(4), 413.

Ponce De León, M. A., and B. N. Bailey (2019), Evaluating the use of Beer's law for estimating light interception in canopy architectures with varying heterogeneity and anisotropy, *ECOL MODEL*, *406*, 133-143.

Reichstein, M., et al. (2005), On the separation of net ecosystem exchange into assimilation and ecosystem respiration: review and improved algorithm, *GLOBAL CHANGE BIOL*, *11*(9), 1424-1439.

Ryu, Y., et al. (2019), What is global photosynthesis? History, uncertainties and opportunities, *REMOTE SENS ENVIRON*, *223*, 95-114.

Schimel, D., et al. (2019), Flux towers in the sky: global ecology from space, *NEW PHYTOL*, *224*(2), 570-584.

Scott, R. L., and J. A. Biederman (2017), Partitioning evapotranspiration using long-term carbon dioxide and water vapor fluxes, *GEOPHYS RES LETT*, *44*(13), 6833-6840.

Shan, N., et al. (2019), Modeling canopy conductance and transpiration from solar-induced chlorophyll fluorescence, *AGR FOREST METEOROL*, *268*, 189-201.

Song, L., et al. (2016), Applications of a thermal-based two-source energy balance model using Priestley-Taylor approach for surface temperature partitioning under advective conditions, *J HYDROL*, *540*, 574-587.

Stoy, P. C., et al. (2019), Reviews and syntheses: Turning the challenges of partitioning ecosystem evaporation and transpiration into opportunities, *BIOGEOSCIENCES*, *16*(19), 3747-3775.

Sun, Y., et al. (2017), OCO-2 advances photosynthesis observation from space via solar-induced chlorophyll fluorescence, *SCIENCE*, *358*(6360), m5747.

Tarantola, S., et al. (2006), Random balance designs for the estimation of first order global sensitivity indices, *RELIAB ENG SYST SAFE*, *91*(6), 717-727.

Tol, C., et al. (2014), Models of fluorescence and photosynthesis for interpreting measurements of solar‐induced chlorophyll fluorescence, *Journal of Geophysical Research: Biogeosciences*, *119*(12), 2312-2327.

Way, D. A., et al. (2014), Increasing water use efficiency along the C3 to C4 evolutionary pathway: a stomatal optimization perspective, *J EXP BOT*, *65*(13), 3683-3693.

Wolf, A., et al. (2016), Optimal stomatal behavior with competition for water and risk of hydraulic impairment, *Proceedings of the National Academy of Sciences*, *113*(46), E7222-E7230.

Wolz, K. J., et al. (2017), Diversity in stomatal function is integral to modelling plant carbon and water fluxes, *NAT ECOL EVOL*, *1*(9), 1292-1298.

Yang, X., et al. (2015), Solar-induced chlorophyll fluorescence that correlates with canopy photosynthesis on diurnal and seasonal scales in a temperate deciduous forest, *GEOPHYS RES LETT*, *42*(8), 2977-2987.

Yang, Y., et al. (2015), An analytical model for relating global terrestrial carbon assimilation with climate and surface conditions using a rate limitation framework, *GEOPHYS RES LETT*, *42*(22), 9825-9835.

Yu, L., et al. (2019), High‐Resolution Global Contiguous SIF of OCO‐2, *GEOPHYS RES LETT*, *46*(3), 1449-1458.

Yuan, W., et al. (2007), Deriving a light use efficiency model from eddy covariance flux data for predicting daily gross primary production across biomes, *AGR FOREST METEOROL*, *143*(3-4), 189-207.

Zeng, Y., et al. (2019), A practical approach for estimating the escape ratio of near-infrared solar-induced chlorophyll fluorescence, *REMOTE SENS ENVIRON*, *232*, 111209.

Zhang, Y., et al. (2014), Estimation of vegetation photosynthetic capacity from space-based measurements of chlorophyll fluorescence for terrestrial biosphere models, *GLOBAL CHANGE BIOL*, *20*(12), 3727-3742.

Zhang, Y., et al. (2018), A global spatially contiguous solar-induced fluorescence (CSIF) dataset using neural networks, *BIOGEOSCIENCES*, *15*(19), 5779-5800.

Zhang, Y., et al. (2019), Coupled estimation of 500 m and 8-day resolution global evapotranspiration and gross primary production in 2002–2017, *REMOTE SENS ENVIRON*, *222*, 165-182.

Zhang, Z., et al. (2020), Reduction of structural impacts and distinction of photosynthetic pathways in a global estimation of GPP from space-borne solar-induced chlorophyll fluorescence, *REMOTE SENS ENVIRON*, *240*, 111722.

Zhou, S., et al. (2014), The effect of vapor pressure deficit on water use efficiency at the subdaily time scale, *GEOPHYS RES LETT*, *41*(14), 5005-5013.

Zhou, S., et al. (2015), Daily underlying water use efficiency for AmeriFlux sites, *Journal of Geophysical Research: Biogeosciences*, *120*(5), 887-902.

Zhou, S., et al. (2018), Water use efficiency and evapotranspiration partitioning for three typical ecosystems in the Heihe River Basin, northwestern China, *AGR FOREST METEOROL*, *253-254*, 261-273.